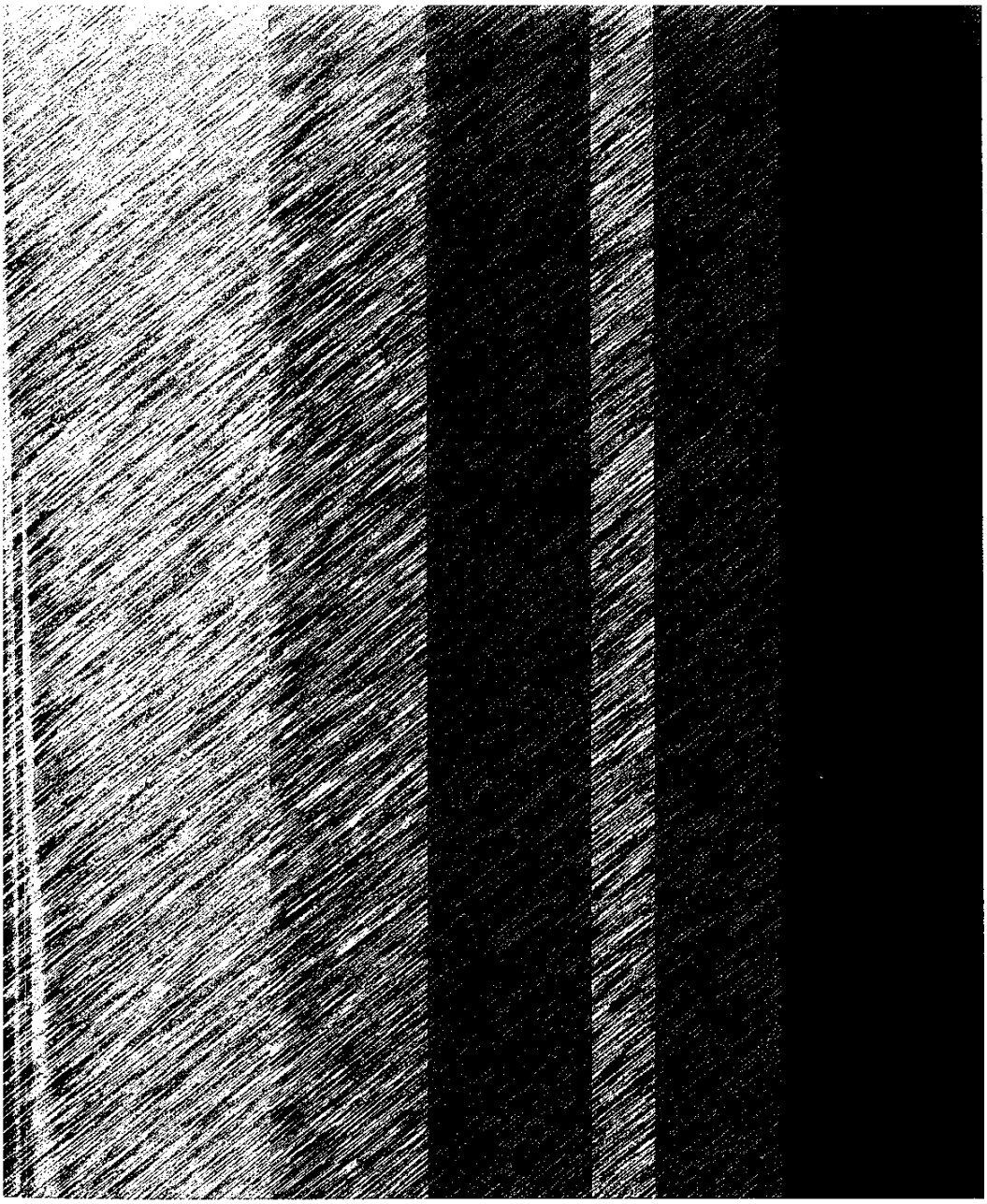

Institution of
MECHANICAL
ENGINEERS

JOURNAL OF

ENGINEERING MANUFACTURE

Including: Short Communications in Manufacture and Design

http://pib.sagepub.com

Influence of carbon content on densification behaviour in forming of sintered plain carbon steel preforms

S Narayan* and **A Rajeshkannan**
School of Engineering and Physics, Faculty of Science, Technology & Environment, The University of the South Pacific, Laucala Campus, Suva, Fiji

The manuscript was received on 2 June 2010 and was accepted after revision for publication on 7 October 2010.

DOI: 10.1177/2041297510393638

Abstract: Complete experimental investigation on the deformation and densification behaviour of sintered plain carbon steel cylindrical preforms with carbon contents of 0, 0.35, 0.75 and 1.1 per cent, under cold upsetting, have been studied in order to understand the influence of various forming parameters such as true axial strain, flow stress, Poisson's ratio, forming limits and formability stress index on the densification process. The above-mentioned powder metallurgy sintered preforms with constant initial theoretical density of 84 per cent and aspect ratio of 0.4 were prepared using a suitable die-set assembly on a 1 MN capacity hydraulic press and sintered for 90 min at 1200 °C. Each sintered preform was cold upset under two different frictional constraints, namely, nil/no and graphite lubricant conditions. Densification–true strain and fracture strain–carbon content relationship was established and presented in this work. Further, attained density is considered to establish flow stress and formability stress index behaviour. The present work provides a guideline for producing P/M components free from open surface pore.

Keywords: densification, fracture strain, Poisson's ratio, formability stress index

1 INTRODUCTION

Powder forging combines powder metallurgy (P/M) and forging technology which has been a versatile and economic technique for manufacturing small intricate and arbitrary alloy combinations. P/M processes provide techno-economic benefits over ingot metallurgy processes; the distinctive features that P/M processes possess being cost reduction, improvement in performance, tailor-made design, greater accuracy, high precision, better surface finish, and homogeneity of structure and the production of unique materials [**1, 2**]. Preforms are prepared in various steps, known as primary deformation processes, which involve powder mixing, compacting and sintering. A known limitation of this route is the residual porosity left in preforms after the sintering process. A secondary deformation process is used in order to enhance the properties of sintered powder materials. Secondary processes such as pressing or re-pressing, powder extrusion, powder rolling, and infiltration can be used to improve the mechanical properties of parts produced through the conventional powder metallurgy route [**3–5**]. The vast application of ferrous powder metallurgy materials of high performance in machine tools, automotive and aerospace industries provides reasons for researchers to analyse powder metallurgy materials behaviour under metal-forming processes and the endeavour of the present researchers is to produce parts to near theoretical density; however, 100 per cent dense components cannot be produced [**6, 7**]. The changing behaviour of the materials and pores

**Corresponding author: School of Engineering and Physics, Faculty of Science, Technology & Environment, The University of the South Pacific, Laucala Campus, PO Box 1168, Suva, Fiji.*
email: narayan_su@usp.ac.fj

during cold upsetting of sintered alloy is dependent on the preform characteristics such as sintered density, pore distribution, preform geometry, and alloying elements. Hence, the prediction of failure in powder preform forging is important from the viewpoint of die design and selection of preform geometry, since the material properties may affect the final shape of a deformed workpiece and may cause defects such as cracks or folds [**8, 9**]. During the elastic deformation of fully dense material, Poisson's ratio remains constant and is a property of the material. The ratio is 0.5 for all materials that conform to volume constancy. However, in the plastic deformation of sintered P/M preforms, density changes occur, resulting in Poisson's ratio being less than 0.5 and tending to approach 0.5 only in the near vicinity of the theoretical density. Since the primary cause of fracture in upsetting is the circumferential tensile stresses, it is therefore essential to investigate fracture during cold upsetting of sintered powder materials [**10**].

Geometrical design of the preform in metal forging of complex parts has great effects on the forging load and plays a key role in improving product quality, such as ensuring a defect-free product and proper metal flow. The formability limit of powder metallurgy material is usually determined by visible crack initiation on the free surface. By careful selection of process parameters and deformation process the densification can be enhanced and the appearance of cracks on the deforming preforms can be avoided by increasing the compressive level of the stresses on the material [**11–13**]. Lubrication also plays an important role in the metal flow particularly in cold upsetting and affects the densification and forming limit mechanisms. A good lubrication improves the quality of the products through the reduction of defects and improvement in the dimensional accuracy and surface finish [**14–16**]. The workability or formability of the P/M material plays a major role in determining whether the P/M material will be formed successfully or fracture initiates in the forming process. Formability is a measure of the extent of deformation to which a material can withstand the induced internal stresses of forming prior to the occurrence of fracture [**17**]. It has been reported [**18, 19**] that the effect of relative density (fractional theoretical density) is a major concern on the formability of P/M material. It is imperative to note that the major concerns for structural applications are the extent to which P/M materials are formed and when maximum density is achieved. Thus, the present investigation aimed to establish the densification behaviour and forming limit of powder metallurgy preforms of pure iron, Fe-0.35%C, Fe-0.75%C and Fe-1.1%C experimentally with the influence of lubricant conditions namely nil/no and graphite lubricant and to establish the technical relationship that exists between the characteristics of densification, fracture strain in the hoop direction and the formability stress index with respect to true height strain. Furthermore, the technical relationship that exists between flow stress, Poisson's ratio and formability stress index with respect to percentage fractional theoretical density was defined. Finally, the fracture strain against percentage carbon content relationship was established for the four powder metallurgy preforms under nil/no and graphite lubricant conditions for 0.4 initial aspect ratio.

2 EXPERIMENTAL DETAILS

2.1 Materials and characterization

Atomized iron powder of less than or equal to 150 μm size and graphite powder of 2–3 μm size were used in the present investigation. Analysis indicated that the purity of iron was 99.7 per cent and the rest were insoluble impurities. The characteristic (apparent density, flowrate and particle size distribution) of iron powder, Fe-0.35%C, Fe-0.75%C, and Fe-1.1%C blends are shown in Tables 1 and 2.

2.2 Blending, compaction, and sintering

A powder mix corresponding to Fe-0%C, Fe-0.35%C, Fe-0.75%C, and Fe-1.1%C was taken in a stainless steel pot with the powder mixed using porcelain balls (10 to 15 mm diameter) with a ratio of 1 : 1 by weight. The pot containing the blended powder was subjected to the blending operation by securely tightening and then fixing it to the pot mill. The mill was operated for 20 h to obtain a homogenous mix.

Table 1 Characterization of iron powder

Si. no.	Property	Iron	Fe-0.35%C blend	Fe-0.75%C blend	Fe-1.1%C blend
1.	Apparent density (g/cc)	3.38	3.37	3.29	3.21
2.	Flow rate, (s/50 g) by Hall flow meter	26.3	28.1	25.3	24.8
3.	Compressibility (g/cm^3) at pressure of 430 ± 10 MPa	6.46	6.26	6.41	6.35

Table 2 Sieve size analysis of iron powder

Sieve size (μm)	150	+125	+100	+75	+63	+45	−45
Wt.% ret.	10.60	24.54	15.46	19.90	11.10	8.40	10.00

Green compacts of 28 mm diameter and 12 mm in length were prepared. The powder blend was compacted on a 1.0 MN hydraulic press using a suitable die, a punch, and a bottom insert in the pressure range of 430 ± 10 MPa to obtain an initial theoretical density of 0.84 ± 0.01. In order to avoid oxidation during sintering and cooling, the entire surface of the compacts were indigenously formed and ceramic coated. These ceramic-coated compacts were heated in the electric muffle furnace at a temperature of 1200 ± 10 °C. At this temperature the compacts were sintered for 90 min followed by furnace cooling.

2.3 Cold deformation

The sintered and furnace-cooled preforms were machined to a suitable dimension to provide a height-to-diameter ratio of 0.40. The initial dimensions of the cylindrical preforms were measured and recorded and used to calculate the initial density. Each specimen was compressively deformed between a flat die-set in the incremental loading step of 0.05 MN using 1 MN capacity hydraulic press under friction conditions, which included dry, unlubricated dies called the nil/no lubricant condition and lubrication consisting of graphite paste (i.e. graphite with acetone) called the graphite lubricant condition. The deformation process was stopped once a visible crack appeared at the free surface. Dimensional measurements such as deformed height and deformed diameters (including bulged and contact) were carried out after every step of deformation using a digital vernier caliper and the density measurements were carried out using the Archi- medes principle. Experimental results were used to calculate the flow stress, true height strain, true diameter strain, percentage theoretical density, formability stress index, and Poisson's ratio.

3 THEORETICAL ANALYSIS

The plastic deformation behaviour of porous metals is influenced by the internal pores, and the analysis of porous metals requires an appropriate yield criterion which should take the pore effect into account. Many researchers over the years have analysed several different yield criteria for sintered powder materials which are based on experimental and theoretical analysis [**20–23**]. A typical theorem is that the plastic deformation occurs when the elasticity strain energy reaches a critical value. The formulation can be written as

$$AJ_2' + BJ_1^2 = Y^2 = \delta Y_0^2 \tag{1}$$

where A, B, δ are yield criterion parameters and are functions of relative density, J_1 is the first invariant of the stress tensor, J_2' is the second invariant of the stress deviator and Y_0 and Y are yield strength of a solid and partially dense material having relative density R, respectively [**20**]. The parameters J_1 and J_2' in the cylindrical coordinate system where the axis represents radial, circular and axial direction can be expressed as follows

$$J_2' = \frac{1}{6}\left[(\sigma_r - \sigma_\theta)^2 + (\sigma_\theta - \sigma_z)^2 + (\sigma_z - \sigma_r)^2\right] \tag{2}$$

$$J_1 = \sigma_r + \sigma_\theta + \sigma_z \tag{3}$$

Here for axisymmetric forging, $\sigma_r = \sigma_\theta$, J_2' and J_1^2 can be written as

$$J_2' = \frac{1}{6}\left(2\sigma_\theta^2 + 2\sigma_z^2 - 4\sigma_\theta\sigma_z\right) \tag{4}$$

$$J_1^2 = 4\sigma_\theta^2 + \sigma_z^2 + 4\sigma_\theta\sigma_z \tag{5}$$

Substituting equation (4) and equation (5) into equation (1) gives

$$\frac{A}{6}\left(2\sigma_\theta^2 + 2\sigma_z^2 - 4\sigma_\theta\sigma_z\right) + B\left(4\sigma_\theta^2 + \sigma_z^2 - 4\sigma_\theta\sigma_z\right) = \delta Y_0^2 \tag{6}$$

Qin and Hua [**21**] has investigated and presented the values for yield criterion parameters based on plastic Poisson's ratio, relative density and flow stress of the matrix material and several yield criteria for sintered powder material were also compared with each other. The following yield criteria parameters are chosen in this research as $A = 2 + R^2$, $B = (1 - R^2)/3$, $\delta = [(R - R_0)/(1 - R_0)]^2$. Equation (6) now can be written as

$$Y_0 = \sigma_{\text{eff}} = \left[\frac{(1 - R_0)^2(\sigma_z^2 - 2\sigma_\theta^2 - R(\sigma_\theta^2 - 2\sigma_\theta\sigma_z))}{(R - R_0)^2}\right]^{0.5} \tag{7}$$

Equation (7) gives the expression for effective stress in terms of cylindrical coordinates.

According to Narayansamy *et al.* [**17**], the hoop stress (σ_θ) under triaxial stress state condition can be determined as

$$\sigma_\theta = \left[\frac{2\alpha + R^2}{2 - R^2 + 2R^2\alpha}\right]\sigma_z \tag{8}$$

where $\alpha = \mathrm{d}\varepsilon_\theta/\mathrm{d}\varepsilon_z$.

The stress formability factor [**18**] is given as

$$\beta = \frac{J_1}{(3J_2')^{0.5}} = \frac{3\sigma_{\text{m}}}{\sigma_{\text{eff}}} \tag{9}$$

where $\sigma_{\text{m}} = (\sigma_r + \sigma_\theta + \sigma_z)/3 = (2\sigma_\theta + \sigma_z)/3$, is the hydrostatic stress.

The stress formability factor as expressed in equation (9) is used to describe the effect of mean stress and the effective stress on the forming limit of P/M compacts in upsetting.

4 RESULTS AND DISCUSSION

4.1 Densification characteristics

Figures 1 and 2 are drawn to show the relationship of fractional theoretical density against true height strain for the nil/no lubricant and graphite lubricant conditions, respectively. The graphs are plotted for different carbon content in the preform with constant aspect ratio of 0.4. The characteristics of the two curves show that with increasing true height strain, densification continuously increased, irrespective of the carbon content in the preform and frictional constraints. Figure 1 follows two different mechanisms of densification. During the first mechanism of deformation, from zero to 0.33 true height strain, it is seen that the densification rate was highest in the pure iron preform and the densification rate decreased with increasing carbon content. However, during the second mechanism of deformation, it is clearly evident from Fig. 1 that the densification rate was the highest in the preform containing 1.1 per cent carbon. Furthermore, the densification rate reduced with

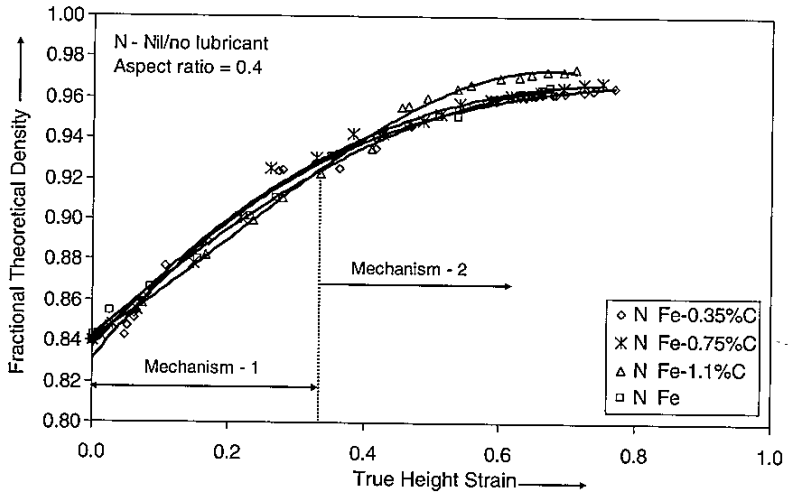

Fig. 1 Influence of carbon content on the densification of sintered plain carbon steel preforms under nil/no lubricant condition

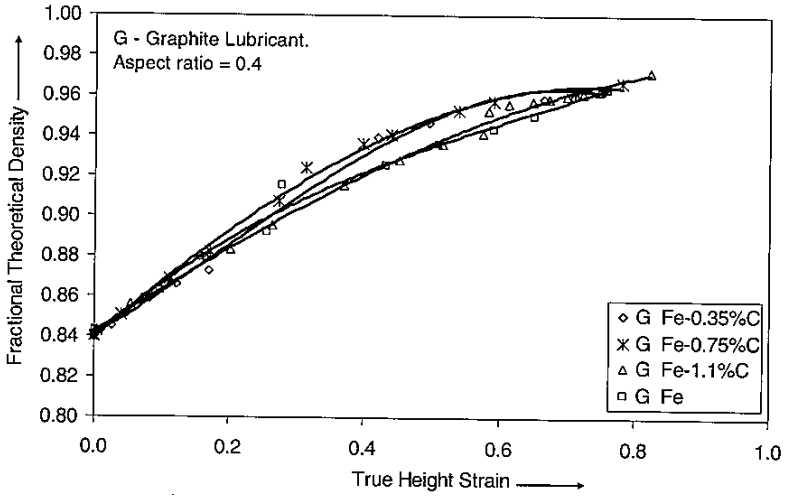

Fig. 2 Influence of carbon content on the densification of sintered plain carbon steel preforms under graphite lubricant condition

reducing carbon content in the preform that was cold deformed under the nil/no lubricant condition. Apart from iron-to-iron bonding, the carbon particles diffused into the ferrous matrix during the sintering process. Another important factor affecting the properties of the sintered steel preform was the combination of carbon with the iron particles. The pore size was affected by the above phenomenon together with shrinkage during the sintering process. As the smaller carbon particle size increased in the preform the pore size reduced and it was difficult to deform their larger size pores; hence, the densification rate was enhanced for pure iron during mechanism 1 as the larger pores were more easily collapsed and closed. Narayanasamy *et al.* [**24, 25**] have presented the microstructure of pure iron, Fe-0.4%C and Fe-0.8%C and it can be seen that as the smaller carbon particle size increased in the preform the pore size reduced. During mechanism 2 lateral deformation was more pronounced than during mechanism 1 and before pore closure, the larger pores present in the pure iron preform elongated in the lateral direction more than the smaller pores present in the iron carbon alloy preform; this was the reason for the enhanced densification rate in the 1.1 per cent carbon preform during mechanism 2 in comparison with mechanism 1. Furthermore, observation of Figs 1 and 2 shows that the densification rate was enhanced in the case of the nil/no lubricant condition in comparison with the graphite lubricant condition; however, the difference in the final density achieved by the preforms was marginally smaller. Hence, it can be said that increasing frictional constraints and increasing carbon content promoted the density and densification rate in the preform during cold axial deformation.

Figures 3 and 4 are drawn to show the relationship of flow stress against fractional theoretical density for nil/no and graphite lubricant conditions, respectively. The graphs are plotted for different carbon content in the preform with constant aspect ratio of 0.4. It can be seen from Figs 3 and 4 that the flow stress was the highest for Fe-1.1%C for any given densification, followed by Fe-0.75%C, Fe-0.35%C and it was lowest for pure iron. The above trend was the same irrespective of the lubricants employed. The smaller carbon particles (2–3 μm) fill the gaps between larger iron particles thereby reducing the pore size in the P/M preform; hence, as the amount of smaller particle size (carbon particles) increases, the pore size in the P/M preform becomes smaller and, therefore, the flow stress required is higher due to higher load requirements for further plastic deformation. Furthermore, observation of the two figures reveal that the nil/no lubricant preforms had better densification characteristics in comparison with the graphite lubricant preforms; however, the effect of the lubricants was only evident during the final stages of deformation. Thus, from Figs 1 and 2 it can be concluded that when the frictional constraints were increased as well as the carbon content, the densification rate can be substantially enhanced.

Figure 5 is drawn to show the relationship of true diameter strain against true height strain for the nil/no lubricant condition. The aspect ratio was kept constant at 0.4. When a fully dense material is deformed, the ratio of lateral deformation to the axial deformation is 0.5 as volume constancy applies and

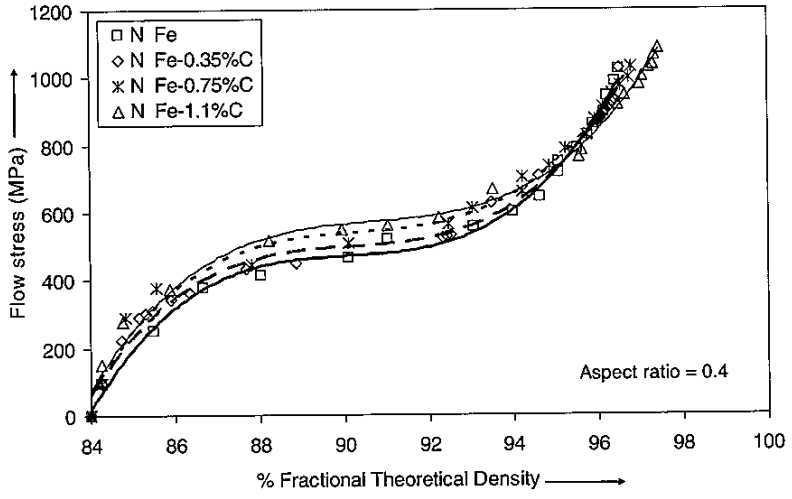

Fig. 3 Influence of carbon content on the relationship between the flow stress and percentage fractional theoretical density of sintered plain carbon steel preforms under nil/no lubricant condition

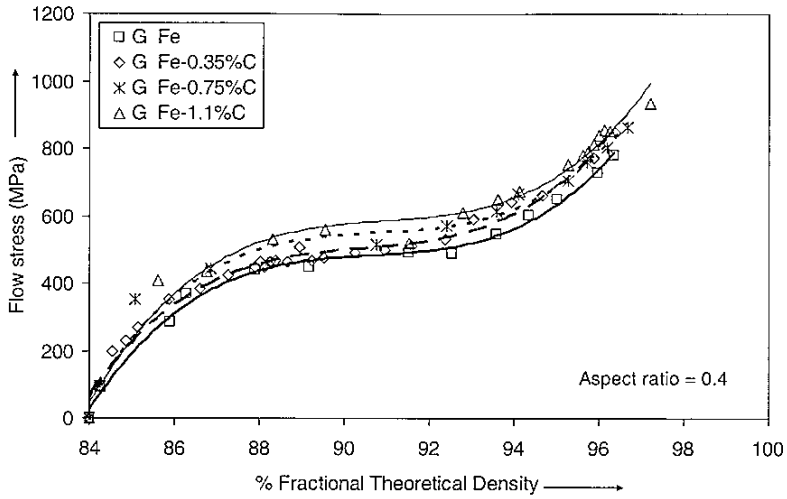

Fig. 4 Influence of carbon content on the relationship between the flow stress and percentage fractional theoretical density of sintered plain carbon steel preforms under graphite lubricant condition

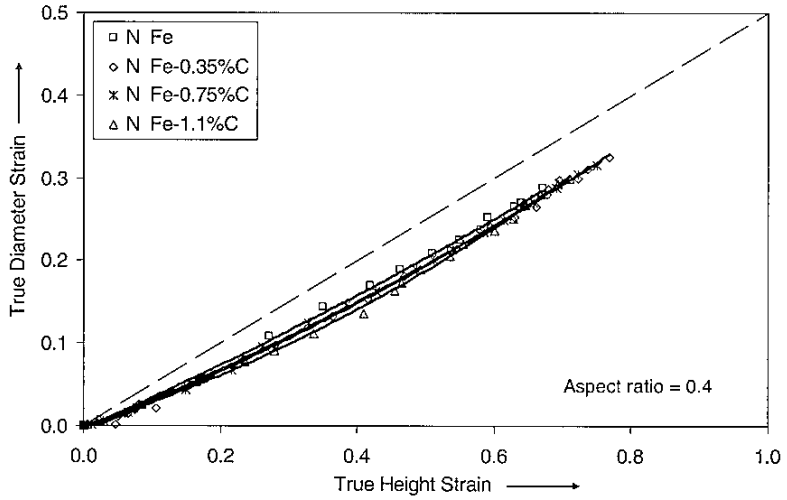

Fig. 5 Relationship between true diameter strain and true height strain with the influence of carbon content

is represented by the dashed line in Fig. 5. However, in the case of a porous material in which volume changes occur during the deformation, closing of pores results in the lateral deformation of a P/M material being less than that of a fully dense material, as is clearly seen in Fig. 5. The curves plotted for porous material were below the dashed line, showing that the Poisson's ratio (ratio of lateral strain to axial strain) in the case of the P/M materials was less than 0.5. Furthermore, Fig. 5 shows that during the final stages of deformation the lines merge and become parallel to the dashed line.

4.2 Poisson's ratio

Figure 6 is drawn to show the relationship of Poisson's ratio against percentage fractional theoretical density for the nil/no lubricant condition under the influence of changing percentages of carbon content in the preforms. The initial aspect ratio was kept constant at 0.4. Irrespective of the percentage carbon content in the preform, the general behaviour of the curves show that the Poisson's ratio increased rapidly with little densification followed by a more gradual increase in the Poisson's ratio values. Furthermore,

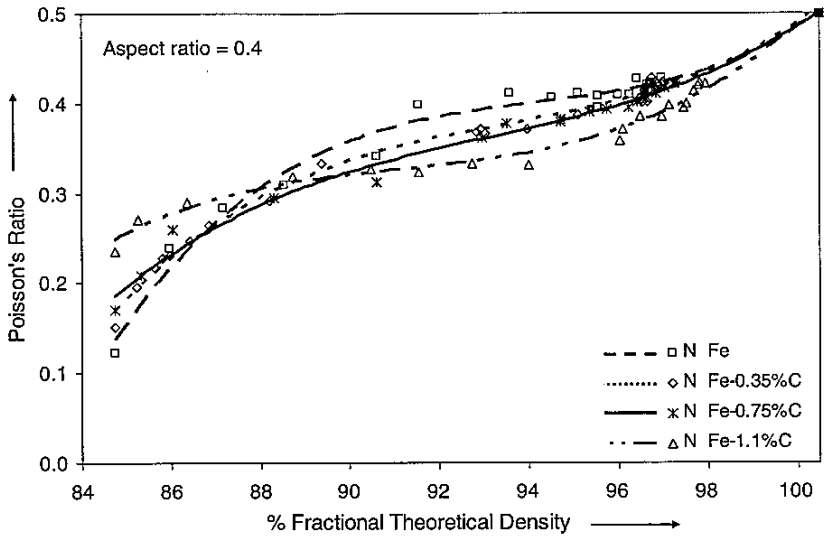

Fig. 6 Variation of Poisson's ratio with per cent fractional theoretical density of sintered plain carbon steel preforms under nil/no lubricant condition

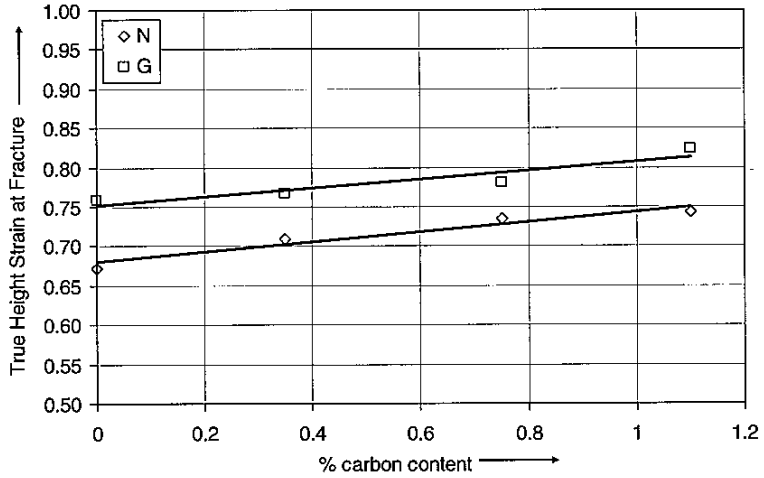

Fig. 7 Relationship between height strain at fracture in cold deformation of sintered plain carbon steel preform with percentage carbon content

Poisson's ratio showed a tendency to a limiting value of 0.5 as densification progressed towards the vicinity of near theoretical density. During the intermediate stage in which most of the densification occurred (87 to 98 per cent theoretical density) the Poisson's ratio values for pure iron were greater in comparison with iron carbon alloys. It can be seen (Fig. 5) that the lateral deformation was enhanced in the case of pure iron in comparison with iron carbon alloy. Poisson's ratio decreased with the increasing amount of carbon content in the preforms; hence it can be said that decreasing the percentage of carbon content in the preform facilitated deformation.

4.3 Forming limit

Figures 7 and 8 show the variation of true height strain at fracture and true diameter strain at fracture, respectively against percentage carbon content under the influence of the nil/no and graphite lubricant conditions. The aspect ratio was kept constant at 0.4. It is clearly evident from Figs 7 and 8 that as the carbon content was increased, the true height strain at fracture and the true diameter strain at fracture was increased. As the carbon content was increased in the preforms the pore size reduced, thereby increasing the grain boundaries. By interfering with dislocation

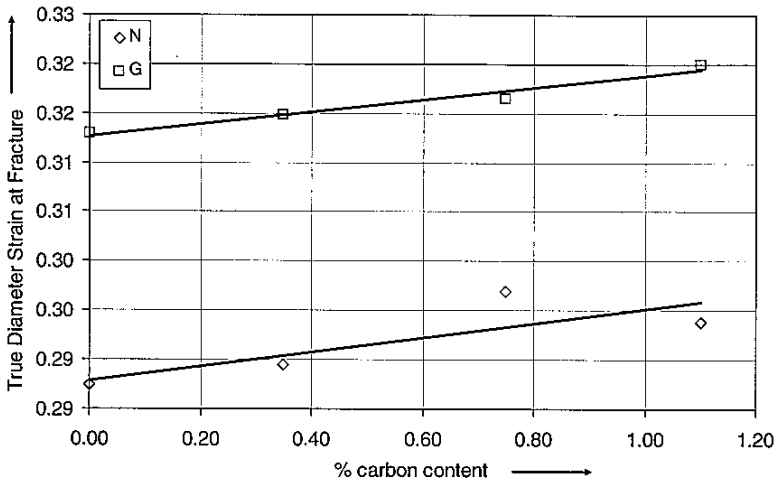

Fig. 8 Relationship between diameter strain at fracture in cold deformation of sintered plain carbon steel preform with percentage carbon content

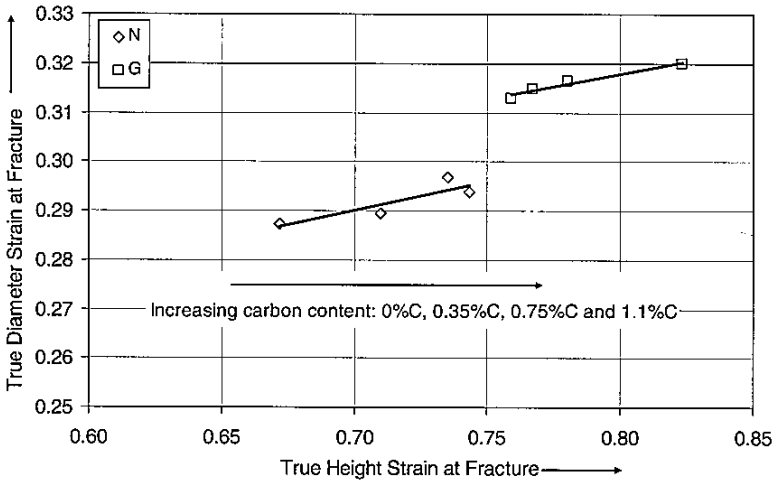

Fig. 9 Relationship between true diameter strain and true height strain at fracture

movement, grain boundaries also contribute to the characteristic property (strain hardening) of a metal causing it to become stronger as it is deformed, thus increasing the height and diameter strain to fracture with increasing carbon content. The frictional condition during cold deformation in the lateral direction induces barrelling in the preform, which is the root cause of the evolution of cracking at the free surface of the preform. Furthermore, the true height strain at fracture and true diameter strain at fracture were enhanced in the case of the graphite lubricant preforms in comparison with the nil/no lubricant preforms; hence the intensity of barrelling increased with increasing frictional constraints and was in good agreement with the results reported by Rajeshkannan *et al.* [9].

Figure 9 shows the relationship of true diameter strain at fracture against true height strain at fracture under the influence of carbon content in the preforms and frictional constraints (nil/no and graphite employed lubricant). The aspect ratio was kept constant at 0.4. It can be seen that the slope of the curves shown in Fig. 9 are almost the same; hence, the effect of increasing the carbon content in graphite lubricant condition in comparison with the nil/no lubricant condition was literally nil. However, the graphite lubricant enhanced the lateral deformation in the preforms. The prediction of failure in the powder preform forging is important from the viewpoint of die design and selection of preform geometry and the above graphs are essential in design.

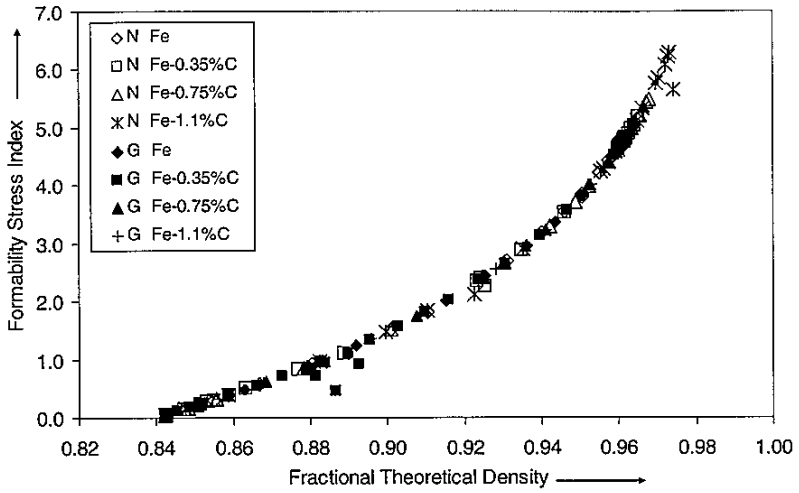

Fig. 10 Relationship between formability stress index and fractional theoretical density for aspect ratio of 0.4

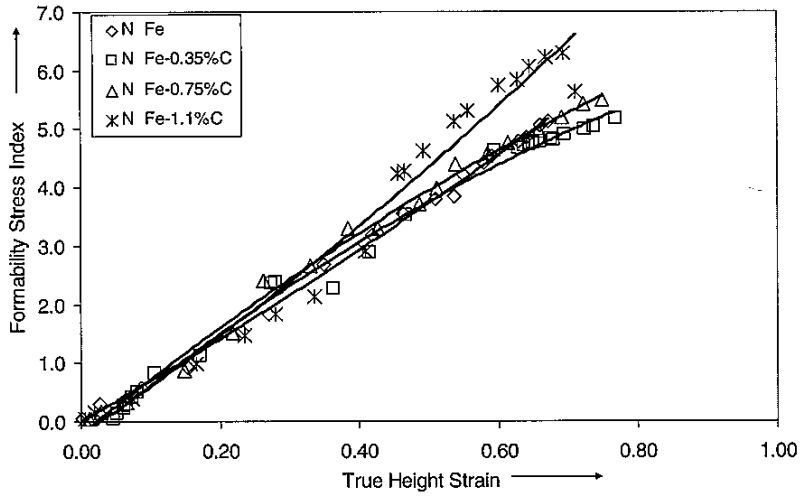

Fig. 11 Relationship between formability stress index and true height strain of sintered plain carbon steel preforms under nil/no lubricant condition

Figure 10 shows the relationship of formability stress index against fractional theoretical density under the influence of carbon content in the preforms and frictional constraints (nil/no and graphite employed lubricant). The aspect ratio was kept constant at 0.4. The characteristic nature of the curves is similar and shows that as the densification increased the formability stress index also increased. As seen from Fig. 10, the effect of carbon content and frictional constraints on the formability stress index rate was literally nil; however, an improved final formability stress index value was observed for Fe-1.1%C preform under the nil/no lubricant condition.

Figure 11 shows the relationship of formability stress index to true height strain under the influence of carbon content. The aspect ratio was kept constant at 0.4 and the preforms were cold upset forged under the nil/no lubricant condition. For all preforms with different carbon contents, the axial strain increased as the value of the formability stress index increased. It can be seen that the formability stress index values decreased with decreasing carbon content in the preform for a given true height strain value. For Fe-1.1%C, the formability stress index showed a very high value at the fracture strain. The finding of a higher formability stress index value for Fe-1.1%C

preform was due to the closure of very fine pores. Furthermore, for pure iron, Fe-0.35%C and Fe-0.75%C the final formability stress index achieved was almost the same, however at different strain values.

5 CONCLUSIONS

From the present investigations it can be seen that both frictional constraints and carbon content had significant implications on the densification. Forming limit mechanisms and the major conclusions that were drawn are listed here.

1. Increasing carbon content in preform and increasing frictional constraints promoted both densification and densification rate. Furthermore, Poisson's ratio showed a tendency to a limiting value of 0.5 as densification progressed towards the vicinity of near theoretical density.
2. Fracture strains in both lateral and axial directions were increased with increasing carbon content and reducing frictional constraints; however, this promotion of densification with reducing frictional constraints should not be taken for granted as this substantial lateral deformation only elongated the voids but did not effectively close them.
3. The effect of carbon content and frictional conditions on the formability stress index rate against promoted density was literally nil but against height strain it was prominent; however, the formability stress index value at fracture strain was highest in the preform containing the highest carbon content.

REFERENCES

1 **Huang, C. C.** and **Cheng, J. H.** An investigation into the forming limits of sintered porous materials under different operational conditions. *J. Mater. Process. Technol.*, 2004, **148**, 382–393.

2 **Chandramouli, R., Pandey, K. S., Kandavel, T. K., Ashokkumar, T.,** and **Shanmugasundaram, D.** Influence of material flow constraints during cold forming on the deformation and densification behaviour of hypoeutectoid P/M steel ring preforms. *Int. J. Adv. Mfg. Technol.*, 2007, **31**, 926–932.

3 **Zhang, X. Q., Peng, Y. H., Li, M. Q., Wu, S. C.,** and **Ruan, X. Y.** Study of workability limits of porous materials under different upsetting conditions by compressible rigid plastic finite element method. *J. Mater. Engng. Perform.*, 2000, **9**, 164–169.

4 **Whang, B. B.** and **Kobayashi, S.** Deformation characterization of powdered compacts in compaction. *Int. J. Mach. Tools Mfg.*, 1990, **30**, 309–323.

5 **Kandavel, T. K., Chandramouli, R.,** and **Ravichandran, M.** Experimental study on the plastic deformation and densification characteristics of some sintered and heat treated low alloy powder metallurgy steels. *Mater. Des.*, 2010, **31**, 485–492.

6 **Lindskog, P.** Economy in car-making – powder metallurgy. In *Business briefing: global automotive manufacturing and technology materials*, 2003, pp. 1–5 (Business Briefings Ltd, London).

7 **Mamalis, A. G., Petrossian, G. L.,** and **Manolakos, D. E.** Limit design of porous sintered metal powder machine elements. *J. Mater. Process. Technol.*, 2000, **98**, 335–342.

8 **Kandavel, T. K., Chandramouli, R.,** and **Shanmugasundaram, D.** Experimental study of the plastic deformation and densification behaviour of some sintered low alloy P/M steels. *Mater. Des.*, 2009, **30**, 1768–1776.

9 **Rajeshkannan, A., Pandey, K. S.,** and **Shanmugam, S.** Some investigation on the cold deformation behaviour of sintered iron-0.8% carbon alloy powder preforms. *J. Mater. Process. Technol.*, 2008, **203**, 542–547.

10 **Narayanasamy, R.** and **Selvalumar, N.** Deformation behaviour of cold upset forming of sintered Al-Fe composite preforms. *J. Engng. Mater. Technol.*, 2005, **127**, 251–256.

11 **C., Gracio, J. J.,** and **Barata da Rocha, A.** An experimental and theoretical analysis on the application of stress-based forming limit criterion. *Int. J. Mech. Sci.*, 2006, **48**, 414–429.

12 **Lee, S. R., Lee, Y. K., Park, C. H.,** and **Yang, D. Y.** A new method of preform design in hot forging by using electric field theory. *Int. J. Mech. Sci.*, 2002, **44**, 773–792.

13 **Sedighi, M.** and **Tokmechi, S.** A new approach to preform design in forging process of complex parts. *J. Mater. Process. Technol.*, 2008, **197**, 314–324.

14 **Rajeshkannan, A.** and **Narayan, S.** Strain hardening behaviour in sintered Fe-0.8%C-1.0%Si-0.8%Cu powder metallurgy preform during cold upsetting. *Proc. IMechE, Part B: J. Engng. Mfg.*, 2009, **223**, 1567–1574. DOI: 10.1243/09544054JEM1587.

15 **Ramesh, B.** and **Senthivelan, T.** Formability characteristics of aluminium based composite-a review. *Int. J. Engng. Technol.*, 2010, **2**, 1–6.

16 **Simchi, A.** Effects of lubrication procedure on the consolidation, sintering and microstructural features of powder compacts. *Mater. Des.*, 2003, **24**, 585–594.

17 **Narayanasamy, R., Ramesh, T.,** and **Pandey, K. S.** Some aspects on workability of aluminium-iron powder metallurgy composite during cold upsetting. *Mater. Sci. Engng. A*, 2005, **391**, 418–426.

18 **Rahman, M. A.** and **El-Sheikh, M. N.** Workability in forging of powder metallurgy compacts. *J. Mater. Process. Technol.*, 1995, **54**, 97–102.

19 **Liu, Y., Chen, L. F., Tang, H. P., Liu, C. T., Liu, B.,** and **Huang, B. Y.** Design of powder metallurgy titanium alloys and composites. *Mater. Sci. Engng. A*, 2006, **418**, 25–35.

20 **Lewis, R. W.** and **Khoei, A. R.** A plasticity model for metal powder forming processes. *Int. J. Plasticity*, 2001, **17**, 1659–1692.

21 **Qin, X. P.** and **Hua, L.** Deformation and strengthening of sintered ferrous material. *J. Mater. Process. Technol.*, 2007, **188**, 694–697.

22 **Sun, X. K., Chen, S. J., Xu, J. Z., Zhen, L. D.,** and **Kim, K. T.** Analysis of cold compaction densification behaviour of metal powders. *Mater. Sci. Engng. A*, 1999, **267**(A), 43–49.

23 **Han, H. N., Oh, K. H.,** and **Lee, D. N.** Analysis of forging limit for sintered porous metals. *Scripta Metallurgica et Materialia*, 1995, **32**, 1937–1944.

24 **Narayanasamy, R., Anandakrishnan, V.,** and **Pandey, K. S.** Effect of carbon content on workability of powder metallurgy steels. *Mater. Sci. Engng. A*, 2008, **494**, 337–342.

25 **Narayanasamy, R., Anandakrishnan, V.,** and **Pandey, K. S.** Effect of carbon content on instantaneous strain-hardening behaviour of powder metallurgy steels. *Mater. Sci. Engng. A*, 2008, **497**, 505–511.

APPENDIX

Notation

C	carbon
Fe	iron
R	relative density
R_o	initial relative density
ε_θ	true hoop strain
ε_z	true axial strain
σ_z	axial stress
σ_θ	hoop stress
σ_r	radial stress
σ_{eff}	effective stress